Causes of Interannual to Decadal Variability of Gila River Streamflow over the Past Century

M. A. Pascolini-Campbell[a], Richard Seager[b], David S. Gutzler[c], Benjamin I. Cook[d], Daniel Griffin[e]

Corresponding author Tel: +1 3473460009

email: map2251@columbia.edu

[a]*Department of Earth and Environmental Sciences, Columbia University, New York, USA.*
[b]*Lamont Doherty Earth Observatory of Columbia University, Palisades, New York, USA.*
[c]*University of New Mexico, Albuquerque, New Mexico.*
[d]*NASA Goddard Institute for Space Studies, New York, USA*
[e]*Woods Hole Oceanographic Institution, Woods Hole, USA*

Abstract

Flow data for the Gila River, New Mexico, shows peaks in the winter-spring (December-January-February-March-April-May), and summer (August-September). Winter flow is typically greater than summer flow, although large spikes are found to appear intermittently in summer values. The mechanisms responsible for the variability of the winter-spring and summer streamflow peaks are investigated by correlation of streamflow with precipitation and sea surface temperature for 1928 to 2012. Decadal variability in the flow record is also examined for a longer term perspective on Gila River streamflow. Results indicate a strong coupling between the winter-spring streamflow and winter-

spring precipitation and winter-spring streamflow and with Pacific SST with El Niño conditions causing increased precipitation and streamflow. Decadal Pacific variability helps explain the transition from high winter flow in the late 20th century to lower flows in the most recent decade. The summer streamflow has a somewhat weaker correlation with summer precipitation and Pacific SST, and its variability is more likely influenced by local variability within the North American Monsoon. Tree ring-based reconstructions of the Palmer Drought Severity Index and the Standardized Precipitation Index indicate much more severe and extended periods of droughts and pluvials in past centuries as well as periods of concurrent winter and summer drought.
Keywords:

streamflow decadal variability; drought; pluvials; treering; teleconnections; North American Monsoon

1. Introduction

[1] The Gila River flows approximately 600 miles west across Arizona, from its headwaters in New Mexico to join the Colorado River just above its mouth. The Gila River receives water from both winter precipitation and the North American Monsoon, producing a complex hydrograph with spring and summer peak flows [14]. The Gila River has been gaged since 1928

and its historical flows show considerable interannual to decadal variability (ibid.). Precipitation and streamflows of other rivers in the Southwest have been shown to be affected by various mechanisms, including responses to Pacific and Atlantic sea surface temperature (SST) anomalies [15, 35, 21]. In addition to the influences of climate variability, aridity in the Southwest United States is projected to intensify with global warming [32, 29] and this will have implications for precipitation and streamflow in the region. Understanding these varying influences on streamflow is vital for producing reliable projections of future streamflows and water resources in the coming decades.

[2] The Gila River is a vital source of water for multiple groups in New Mexico and Arizona including farmers, industries, and local communities including the Gila River Indian Community (Oglesby, 2011). It supplies water to Catron, Grant, Hidalgo and Luna Counties, New Mexico, for varied purposes including agriculture (which accounts for 86 percent of water consumption in the state [20]) , commercial use, industry, mining and power extraction. The Gila River is also the subject of an ongoing debate on planning for water use in New Mexico as allowed under the Arizona Water Settlements Act (AWSA). The social importance of the river motivates the need

for improved scientific understanding of the mechanisms responsible for its flow.

[3] Here we present the first comprehensive study of historical Gila River flow variability. Since the river is fed by 1) snowmelt in the spring and 2) the North American Monsoon in the summer, attention must focus on both winter and summer season climate variability. Many previous studies have demonstrated the connection between Southwest precipitation during the winter and Pacific Ocean SST anomalies [23, 3, 30]. This connection is primarily due to the El Niño-Southern Oscillation (ENSO) [3], a coupled atmosphere-ocean phenomenon with equatorial Pacific SST varying at the 2 to 7 year timescale and being strongest during the winter (December-January-February (DJF)) season (e.g. [39]). Those studies found that winters of warm SST anomalies (El Niño events) precede higher than average spring streamflow and precipitation in southwest North America, and periods of cold SST anomalies (La Niña events) tended to go along with low precipitation and streamflow [3]. Focusing on precipitation variability, modeling studies have also indicated the importance of Pacific SST anomalies in generating persistent, multiyear, droughts and pluvials in North America [28, 31], and multidecadal precipitation variability [29].

[4] From Mexico into the southwestern U.S., the North American Monsoon brings a summer (July-August-September (JAS)) peak in rainfall [1, 2] and Monsoon variability presumably can also drive streamflow variability, including of the Gila. Modeling studies have indicated that greenhouse gas (GHG) warming could delay both Monsoon onset and retreat [34, 4] though changes in the Monsoon by region have not yet been closely examined. In addition, the role of increased temperature and potential evapotranspiration rates is predicted to have an impact on the hydrology of the region, adding a further dimension to streamflow change in the future [17, 14].

[5] This study will investigate historical variability of Gila River flow, the nature of the double peaked hydrograph, and in particular the association of flow to SST anomalies in the Pacific and Atlantic Oceans. Key questions addressed will include: 1) precipitation variability in which months best explains the variability of the two peak streamflows?, 2) how are precipitation over the basin and streamflow related to SST anomalies?, 3) what is the relationship of flow variability to ENSO?, and 4) what is the nature and cause of the decadal variability of Gila River flow since 1928. Future climate change impacts on Gila River flow are not examined here (but see [14]). Instead we use observations to explain the past flow variability as one necessary step to

understanding its potential present and future predictability.

2. Data and Methodology

[6] To investigate streamflow and climate variability four observational datasets for the time period of 1928 to 2012 are used. This time span is used as the base period from which climate anomalies are calculated. For streamflow we use mean daily values for the upper Gila River from United States Geological Survey (USGS) Gage Data (in units of cubic meters per second (c.m.s.)) (USGS gage 09430500) (available online at http://waterdata.usgs.gov/usa/nwis/uv094 For precipitation we use two datasets: the first is from the Global Precipitation Climatology Center (GPCC) (in units of mm/month on a 0.5°x0.5° global grid) which is used for generating data over North America for 1928 to 2010 (Schneider et al., 2011). The second precipitation dataset used is from the Parameter Regression on Independent Slopes Model (PRISM; in units of mm/month on a 4km grid), which uses a well-verified, terrain-sensitive algorithm to interpolate between available stations over the period 1895-present [9]. To focus on watershed specific variability, PRISM data was extracted for the Upper Gila Basin (U.S.G.S. Hydrologic Unit Code 150400) using the Westmap internet tool (http://www.cefa.dri.edu/Westmap/). The

interpolation between stations in the PRISM data is sensitive to elevation changes, which is important given the varying topography of our study region. For SST, ERSST V3 reanalysis data (in units of degrees Celsius on a 2°x2° global grid) are used [36]. A reconstruction of the Palmer Drought Severity Index (PDSI) for the United States, based on tree ring data within the North American Drought Atlas (NADAV2a) , is used since 1000 A.D. [5, 6, 7]. Season-specific moisture variability in the pre-instrumental era was assessed with tree-ring reconstructions to create the Standardized Precipitation Index (SPI) for the 7-month season ending in April and the 3-month season ending in August for 1530 to 2008 [13]. For evapotranspiration, precipitation and temperature output is used from the Global Land Data Assimilation System (GLDAS) Common Land Model (CLM) (1979 to 2000) [24], the Variable Infiltration Capacity (VIC) hydrological model (1929 to 2003) [19] as well as NCEP-NCAR CDAS-1 Reanalysis data (1948 to 2012) [18] ((in units of kg/m^2/s for precipitation and evapotranspiration, and degrees Celsius for temperature, on a 1°x1° global grid). The Variable Infiltration Capacity (VIC) hydrological model is also used for evapotranspiration, precipitation and temperature from 1929 to 2003 [19] .The GPCC precipitation, SST and PDSI datasets are available online at the International Research Institute Institute for Climate and Society (IRI) data library (http://iridl.ldeo.columbia.edu/).

[7] To investigate precipitation variations over the Gila River Basin, a time series is constructed from the PRISM data for the Upper Gila Hydrological Unit. Regions affected by the North American Monsoon have been found to contain large degrees of spatial heterogeneity in rainfall and temperature trends, related to the spatially varying nature of convective cloud activity [11] , making it important to examine links between Gila River flow and precipitation on the scale of the basin itself. Consistently stronger correlation between precipitation and streamflow was found to exist when using the PRISM Upper Gila Hydrological Unit Precipitation compared with a rectangular box containing the Gila River catchment upstream of the gage (spanning 108.5°W to 111.5°W and 31.5°N to 33.5°N). Pacific Ocean SST variability related to ENSO is investigated using the Niño-4 index, which is the SST anomaly averaged over the area bound by 5°N to 5°S and 150°W to 160°E. Composites of precipitation over North America corresponding to cold and warm events in the Niño-4 region are also created. Warm (cold) events are identified as those in which the value of the Niño-4 index for DJF season has an anomaly greater (less) than 0.5°C.

[8] A hydrograph for the Gila River is created using streamflow data to determine the magnitude and timing of the dual peaks (as carried out by Gutlzer (2013)). Following identification of the peak months of streamflow, a cross-correlation with PRISM precipitation is performed to determine for which months the precipitation is best correlated to flow. The timeseries of streamflow and precipitation for these months were then correlated with SST for 1928 to 2012 to create maps of correlation coefficients showing which ocean regions have the greatest influence on Gila River precipitation and flow.

[9] High and low spring streamflow events are then investigated. High events are identified by determining years in which the magnitude of DJF-MAM streamflow is greater than 85 percent of the annual mean, and low events when flow is less than 15 percent of the annual mean for 1928 to 2012. Composites of GPCC precipitation and SST patterns for the high and low events are created to examine co-existing patterns. GPCC data are used for precipitation in this case as they provide global coverage and can be used to illustrate patterns across the entire North American continent.

[10] Decadal variability is investigated through analysis of the timeseries for 1928 to 2012. Composites for GPCC precipitation and SST are created for years of persistently high and low flow to determine the nature of the as-

sociated climatic patterns. PDSI data are compared with JFM precipitation over the Gila Basin, for the period 1928 to 2003. In addition the two dendroclimatological time series are analyzed to examine longer term variability in the region.

3. Results

[11] The box plot (Figure 1a) shows that peak streamflow occurs during the months December-January-February-March-April-May (DJFMAM) and the summer peak occurs during August-September (AS). For these months streamflow reaches monthly mean magnitudes of approximately 5.6 in winter-spring and 2.7 c.m.s. in summer. Figure 1 also shows timeseries of streamflow averaged over the water year (October to September) (Figure 1b), winter-spring (DJFMAM) (Figure 1c) and summer months (AS) (Figure 1d). The timeseries for water year flow (Figure 1b) indicate a high flow period from about 1975 to about 1990, and low flow from about 1945 to about 1960. In addition there is substantial interannual variability in monthly flow throughout the record. There is also a large degree of variability on an annual timescale shown in the box plot of Figure 1a. DJFMAM flow is greater than AS flow, comprising approximately 61 percent of the total mean annual flow

compared to 15 percent over the time period 1928 to 2012. However, certain years exist where the AS flow exhibits sharp spikes which far exceed the DJFMAM flow, notably 1988 and 2006 in which AS flow accounts for 55 and 66 percent of the annual mean flow respectively (Figure 2). The mean cumulative flow was found to be 140 million cubic meters per year, with a maximum mean flow of 13 c.m.s. (occurring in December), and a minimum mean flow of 1.2 c.m.s. (occurring in June).

[12] As can be seen in Figure 1 the distributions of winter-spring and summer flow are positively skewed, and for this reason subsequent analysis is performed using log-transformed flow data. The timeseries for log-transformed DJFMAM and AS streamflow over the time period 1928 to 2012 were then cross-correlated (using Pearson correlation) with PRISM precipitation, first by month and then by season (Figure 3). For the monthly analysis, DJFMAM streamflow was found to correlate best with the preceding winters precipitation, obtaining a maximum correlation coefficient in December of $r = 0.70$ ($p < 0.000$) (Figure 3a). The lag of flow behind precipitation is consistent with winter precipitation falling as snow and being stored in the basin until spring snowmelt. The seasonal correlation between DJFMAM log-transformed streamflow and winter average (NDJFMAM) precipitation

is even higher with a value of r = 0.91 ($p < 0.000$). For monthly analysis of AS log-transformed streamflow, the highest correlation with precipitation is found for the preceding and coincident months of July-August-September (JAS) reaching a maximum value of r = 0.52 ($p < 0.000$) in August (Figure 4b). The seasonal correlation coefficient between JAS precipitation and AS log-transformed flow gave a value of r= 0.77 ($p < 0.000$). The lack of any lag between precipitation and flow is because summer precipitation falls as rain with little storage in the basin. Timeseries for DJFMAM and log-transformed flow with NDJFMAM PRISM precipitation and NDJF SST anomalies in the Niño 4 region for 1928 to 2012 show the coupling of winter-spring flow with both precipitation and Pacific Ocean climatology (Figure 4a, b). The weaker correspondence of AS log-transformed flow with JAS precipitation and Niño-4 SST anomalies is also demonstrated (Figure 4c, d).

[13] PRISM precipitation for the Upper Gila Hydrological Unit in NDJFMAM as well as log-transformed DJFMAM streamflow is correlated with GPCC precipitation over North America (Figure 5a,b). The largest correlation coefficients (aside from the region directly over or adjacent to the Gila River basin) are found to occur across all of southwestern North America including the southern (values of approximately 0.5) and central Plains (also

with a value of approximately 0.5). Negative correlation coefficients stretch inland from the Pacific Northwest. This pattern of positive and negative correlations is a typical ENSO pattern [26, 27, 25]. The JAS PRISM precipitation and the log-transformed AS streamflow is correlated with JAS GPCC precipitation over the region of Gila River watershed (Figure 5c,d). These maps demonstrate the localized nature of summer flow which is consistent with local-scale convective precipitation.

[14] Streamflow during the peak months, and PRISM precipitation for the preceding NDJFMAM and JAS, were then correlated with global SST anomalies for JFM and JAS, respectively (Figure 6c, d). This is based on the assumption that there should be little lag between SST anomalies and the resulting atmospheric circulation anomalies that cause precipitation anomalies. The results show a positive correlation with SSTs in the ENSO region for DJFMAM streamflow and NDJFMAM precipitation with correlation coefficients reaching approximately 0.5. The greatest correlation coefficients appear to occur in the Niño-4 region. The SST correlation pattern extends from the west coast of South America to about the dateline, with cool waters to the north and south in the classic boomerang shape, all features typical of ENSO warm phase anomalies [39]. A similar southwestern North

American precipitation response to tropical SST has been documented in previous studies using Empirical Orthogonal Function and Principal Component analysis [42, 8]. Composites of North American precipitation during NDJFMAM for years of warm and cold SST anomalies in the Niño-4 regions are shown in Figures 6a and b. During anomalously warm years in the Niño-4 region, positive precipitation anomalies occur over southern North America and Mexico. Negative precipitation anomalies are found over the Southwest region corresponding to the Gila River basin during anomalously cold years.

[15] Years of high streamflow are defined as years in which the streamflow value in DJFMAM flow is 85 percent or greater than the annual mean flow (4 events identified), or less than 15 percent for low flow years (3 events identified) over 1928 to 2012. Figure 7a illustrates a GPCC precipitation composite for the high streamflow years. This demonstrates positive precipitation anomalies over the West coast of the U. S., the Gulf region, the U.S. East coast and over Mexico. This pattern of precipitation anomalies is similar to that expected during an ENSO warm phase [26]. A composite of JFM SST anomalies (Figure 7c) for these high streamflow years shows weak warm anomalies in the central tropical Pacific region. This resembles El Niño conditions but the pattern in the eastern tropical Pacific is not typ-

ically El Niño-like in that there are cool off-equatorial SST anomalies. The low streamflow years have below normal precipitation anomalies (Figure 7b) over southwest North America and above normal on the northwest coast of the United States. The SST anomalies for the low flow composite are La Niña like.

[16] Decadal variability is investigated in Figures 8, with years of high streamflow taken as 1977 to 1997 (after the 1977 climatic shift in the Pacific) (Figure 8b,e), and low streamflow as 1945 to 1960 (Figure 8a,d). These different time periods for high and low flow are selected based on analysis of the 10-year running mean of the timeseries for Gila River streamflow from 1928 to 2012 in Figure 1b - d. Decadal trends are particularly apparent in the annual average for streamflow shown in Figure 1b, with a mean value of 6 c.m.s. occurring for the years 1977 to 1997 and 3 c.m.s. for the low flow years of 1945 to 1960. The most recent period, 1999 to 2012, is also investigated (Figure 8c,f). During the high streamflow period (Figures 8a,d) positive precipitation anomalies are observed over southwestern North America and the Gulf Region. This pattern again resembles the El Niño related precipitation anomaly pattern over North America. Consistently, positive SST anomalies occur in the central and eastern Pacific within a meridionally broad pat-

tern resembling decadal El Niño variability [43]. A region of negative SST anomalies is also found to occur in the North Atlantic region. For the low streamflow years (Figures 8b,e) negative precipitation anomalies occur over southwest North America, the coastal southeast U.S. and the Gulf region. Positive anomalies occur over the northwest and much of the eastern U.S. However the SST anomalies in the Pacific and Atlantic Oceans do not clearly show any climate mode pattern. The most recent decade (Figure 8c,f) shows positive precipitation anomalies over the north west United States, and negative anomalies over the south west and Gulf Region. Pacific Ocean SST has generally warm anomalies in the tropics but cold anomalies in the central Pacific. [16] and [33] have shown using SST-forced atmosphere models how a shift in the late 1990s to this SST pattern induced drying across southwest North America.

[17] The Upper Gila Watershed is surrounded by a dense network of moisture sensitive tree-ring chronologies that offer a high-quality and long-term perspective on moisture variability in the centuries prior to the instrumental era. The June-August PDSI reconstruction from the North American Drought Atlas [7]; Figure 9b) illustrates that in the Upper Gila Basin, persistent pluvials centered on the 1910s and 1980s, made the 20th Century per-

haps the wettest of the last millenium. It also highlights protracted drought events previously described in the late 16th century (e.g. [38]) , and several "megadroughts" of the late Medieval Era (e.g., [22, 6, 40]). The anomalously wet 20th century, 16th century "megadrought," and another multi-decadal drought event in the early 1400s are also evident in an unpublished reconstruction of water year flow on the Gila River downstream at Safford Arizona, which covers the period 1332-2005 A.D. [Meko and Hirschboeck, http://treeflow.info/loco/gila.html].

[18] A novel perspective on paleomonsoon precipitation variability in this region is available from summer-forming tree-ring "latewood" [12]. Latewood chronologies have been used to reconstruct June-August standardized precipitation indices for a large area of Arizona and western New Mexico [13]. In the Southwestern U.S., precipitation influence on the summer PDSI is dominated by the cool season [37] and for data in the present study, the relationship between summer PDSI with previous NDJFMAM PRISM precipitation ($r=0.42, p<0.000$) is greater than that with the monsoon (JAS) precipitation (not significant). The summer PDSI is also found to correlate greater with the winter-spring SPI index over 1530 to 2003 ($r = 0.47$, $p<0.000$) than with the summer SPI (not significant). The SPI demonstrates synchronous pe-

riods of negative SPI index between the winter-spring (October-April) and summer around 1575, 1675, 1775, 1825,1880, and 1950 among other periods (although in general the correlation between the two is insignificant). This supports recent Southwestern studies using latewood which find that major decadal droughts of the last several centuries were likely characterized by precipitation deficits during both seasons [38, 10, 41, 13].

[19] While the summer (AS) season correlation between Gila streamflow and basin precipitation is still quite high ($r=0.52$, $p< 0.000$), it is lower than in winter and to explain this the relationship of summer flow with evapotranspiration and temperature from the GLDAS CLM, VIC models and NCEP-NCAR reanalysis output averaged over the Gila River Basin (spanning 108.5W to 111.5W and 31.5N to 33.5N) was also investigated. Results from these studies (not shown) indicate weak correlations between AS summer flow and evaporation, temperature and precipitation - evaporation. Weak correlation is also found to exist between these variables amongst the different models and datasets which calls into question the validity of the evapotranspiration data. An additional analysis for the longer time period July-August-September-October-November as well as considering data for a smaller area corresponding to the watershed, were also performed to capture

all basin storage but this did not improve the correlations.

4. Conclusion

[20] We have presented the first comprehensive analysis of the climatic causes of Gila River flow variability over the time period 1928 to 2012. The Gila River experiences two peaks in its hydrograph: one in the winter to spring (DJFMAM) with a monthly mean magnitude of approximately 5.6 c.m.s, and a second, smaller, peak (about 2.7 c.m.s) in the summer (AS) coinciding with the North American Monsoon The DJFMAM streamflow peak correlates the greatest with precipitation in the preceding NDJFMAM months, with the delay being consistent with winter precipitation falling as snow in the headwaters and moving into the river in spring following snowmelt. The AS streamflow peak correlates the greatest, but at a lower value, with JAS precipitation, the lack of any appreciable lag being consistent with Monsoon precipitation falling as rain and moving quickly into the river. Correlation and composite analyses show that DJFMAM streamflow and NDJFMAM precipitation are positively related to an ENSO like pattern of Pacific SST anomalies. These relations hold in general for individual year examples of high and low spring flows. In contrast, AS streamflow

and precipitation does not have an association to Pacific SST. The weaker link between AS streamflow and summer precipitation, and between summer precipitation and SST anomalies, indicates future studies are needed focused on North American Monsoon variability and the role of other controls on streamflow such as temperature variability. In addition the Gila River basin is affected by highly localized climate variability involving the monsoon and convective storms, particularly during the summer months, requiring analysis to also be performed at the mesoscale.

[21] The Gila River flow also has impressive variability on decadal timescales. This can be explained in large part by decadal ENSO-like variability with the composite for the high flow decades of 1975 to 1990 clearly revealing the warm phase of Pacific decadal variability. The post 1990s decline in Gila River flow is also explained in terms of the shift to cooler tropical Pacific SSTs. The reconstructed PDSI and SPI indexes for past centuries demonstrate prolonged droughts and pluvials as well as periods of synchronous summer and winter dry periods.

[22] The history of the spring maxima of Gila River flow can therefore be largely explained in terms of natural precipitation variability forced by interannual to decadal ENSO variability. This should allow some useful seasonal

to interannual predictabilty of spring Gila River flows. The high flows in the late 20th Century are associated with the warm phase of Pacific decadal variability and the recent downturn in the 21st Century is consistent with the more generally cold tropical Pacific conditions since the 1997/98 El Niño. As the current century evolves, Gila River flow will no doubt be influenced by human-induced climate change but natural variability such as that identified here will also continue. Projections of future Gila River flows, and its important contribution to southwest water resources, will need to account both for the natural variability and the response to human-induced climate change. This work was supported by NSF award AGS-1243204 and NOAA award NA10OAR4310137 “Linking near-term future changes in weather and hydroclimate in western North America to adaptation for ecosystem and water management”. LDEO contribution number XXXX. We thank Jennifer Nakamura and Naomi Henderson for invaluable help preparing the figures. We thank Andrea Ray for useful comments on the manuscript.

[1] Adams, D. K., Comrie, A. C., 2014/04/18 1997. The North American Monsoon. Bulletin of the American Meteorological Society 78 (10), 2197–2213.
URL http://dx.doi.org/10.1175/1520-0477(1997)078<2197:TNAM>2.0.CO;2

[2] Barlow, M., Nigam, S., Berbery, E., 1998. Evolution of the North American Monsoon System. Journal of climate 11 (9), 2238–2257.

[3] Cayan, D., Redmond, K., Riddle, L., 1999. ENSO and hydrologic extremes in the western United States (vol 12, pg 2881, 1999). Journal of climate 12 (12), 3516–3516.

[4] Cook, B. I., Seager, R., 2013. The response of the North American Monsoon to increased greenhouse gas forcing NA MONSOON AND GHG WARMING. Journal of geophysical research. Atmospheres 118 (4), 1690–1699.

[5] Cook, E., Lall, U., Woodhouse, C., Meko, D., 2004. Cook et al. 2004 north american pdsi reconstructions. NOAA Paleoclimatology.

[6] Cook, E. R., Seager, R., Cane, M. A., Stahle, D. W., 2007. North american drought: Reconstructions, causes, and consequences. Earth-science reviews 81 (1-2), 93–134.

[7] Cook, E. R., Seager, R., Heim, R. R., Vose, R. S., Herweijer, C., 2010. Megadroughts in North America: placing IPCC projections of hydroclimatic change in a long-term palaeoclimate context. Journal of quaternary science 25 (1), 48–61.

[8] Dai, A., 2013. The influence of the inter-decadal Pacific oscillation on US precipitation during 1923–2010. Climate dynamics 41 (3-4), 633–646.

[9] Daly, C., Halbleib, M., Smith, J. I., Gibson, W. P., Doggett, M. K., 2008. Physiographically sensitive mapping of climatological temperature and precipitation across the conterminous united states. International journal of climatology 28 (15), 2031–2064.

[10] Faulstich, H. L., Woodhouse, C. A., Griffin, D., 2013. Reconstructed cool- and warm-season precipitation over the tribal lands of northeastern Arizona. Climatic change 118 (2), 457–468.

[11] Gebremichael, M., Vivoni, E. R., Watts, C. J., Rodriguez, J. C., 2007. Submesoscale spatiotemporal variability of North American monsoon rainfall over complex terrain. Journal of climate 20 (9), 1751–1773.

[12] Griffin, D., Meko, D. M., Touchan, R., Leavitt, S. W., Woodhouse, C. A., 2011. LATEWOOD CHRONOLOGY DEVELOPMENT FOR SUMMER-MOISTURE RECONSTRUCTION IN THE US SOUTHWEST. Tree-ring research 67 (2), 87–101.

[13] Griffin, D., Woodhouse, C. A., Meko, D. M., Stahle, D. W., Faulstich, H. L., 2013. North American monsoon precipitation reconstructed

from tree-ring latewood NA MONSOON PRECIPITATION RECONSTRUCTION. Geophysical research letters 40 (5), 954–958.

[14] Gutzler, D. S., in preparation. Streamflow Projections for the Upper Gila River. in preparation.

[15] Gutzler, D. S., Kann, D., Thornbrugh, C., 2002. Modulation of ENSO-Based Long-Lead Outlooks of Southwestern U.S. Winter Precipitation by the Pacific Decadal Oscillation. Weather and forecasting 17 (6), 1163–1172.

[16] Hoerling, M., Quan, X.-W., Eischeid, J., 2009. Distinct causes for two principal u.s. droughts of the 20th century. Geophysical research letters 36 (19).

[17] Hurd, B. H., Coonrod, J., 2008. Climate change and its implications for New Mexico's water resources and economic opportunities. NM State University, Agricultural Experiment Station, Cooperative Extension Service, College of Agriculture and Home Economics.

[18] Kalnay, E., Kanamitsu, M., Kistler, R., Collins, W., Deaven, D., 1996. The NCEP/NCAR 40-Year Reanalysis Project. Bulletin of the American Meteorological Society 77 (3), 437–471.

[19] Liang, X., 1994. A two-layer variable infiltration capacity land surface representation for general circulation models. Thesis (PH.D.)-University of Washington.

[20] Liverman, D., Merideth, R., 2002. Climate and society in the US Southwest: the context for a regional assessment. Climate research 21 (3), 199–218.

[21] McCabe, G., Palecki, M., Betancourt, J., 2004. Pacific and Atlantic Ocean influences on multidecadal drought frequency in the United States. Proceedings of the National Academy of Sciences - PNAS 101 (12), 4136–41.

[22] Meko, D. M., Woodhouse, C. A., Baisan, C. A., Knight, T., Lukas, J. J., Hughes, M. K., Salzer, M. W., 2007. Medieval drought in the upper colorado river basin. Geophysical Research Letters 34 (10).

[23] Molles, M. C., Dahm, C., 1990. A Perspective on El Nino and La Nina: Global Implications for Stream Ecology. Journal of the North American Benthological Society 9 (1), 68–76.

[24] Rodell, M., Houser, P., Jambor, U., Gottschalck, J., Mitchell, 2004.

The Global Land Data Assimilation System. Bulletin of the American Meteorological Society 85 (3), 381–394.

[25] Ropelewski, C. F., Halpert, M., 1996. Quantifying Southern Oscillation-Precipitation Relationships. Journal of climate 9 (5), 1043–1059.

[26] Ropelewski, C. F., Halpert, M. S., 1986. North American Precipitation and Temperature Patterns Associated with the El Niño/Southern Oscillation (ENSO). Monthly weather review 114 (12), 2352–2362.

[27] Ropelewski, C. F., Halpert, M. S., 1989. Precipitation Patterns Associated with the High Index Phase of the Southern Oscillation. Journal of climate 2 (3), 268–284.

[28] Schubert, S. D., Suarez, M., Pegion, P., Koster, R., Bacmeister, J., 03 2004. On the cause of the 1930s dust bowl. Science (New York, N.Y.) 303 (5665), 1855–1859.

[29] Seager, R., Goddard, L., Nakamura, J., Henderson, N., Lee, D. E., 2014. Dynamical Causes of the 2010/11 Texas–Northern Mexico Drought*. Journal of hydrometeorology 15 (1), 39–68.

[30] Seager, R., Harnik, N., Robinson, W., Kushnir, Y., Ting, M., 2005.

Mechanisms of ENSO-forcing of hemispherically symmetric precipitation variability. Quarterly journal of the Royal Meteorological Society 131 (608), 1501–1527.

[31] Seager, R., Kushnir, Y., Herweijer, C., Naik, N., Velez, J., 2005. Modeling of Tropical Forcing of Persistent Droughts and Pluvials over Western North America: 1856–2000. Journal of climate 18 (19), 4065–4088.

[32] Seager, R., Ting, M., Held, I., Kushnir, Y., Lu, J., 2007. Model projections of an imminent transition to a more arid climate in southwestern North America. Science (New York, N.Y.) 316 (5828), 1181–4.

[33] Seager, R., Vecchi, G. A., 12 2010. Greenhouse warming and the 21st century hydroclimate of southwestern north america. Proceedings of the National Academy of Sciences - PNAS 107 (50), 21277–21282.

[34] Seth, A., Rauscher, S. A., Biasutti, M., Giannini, A., Camargo, S. J., 2013. Cmip5 projected changes in the annual cycle of precipitation in monsoon regions. Journal of climate 26 (19), 7328–7351.

[35] Sheppard, P., Comrie, A., Packin, G., Angersbach, K., Hughes, M., 2002. The climate of the US Southwest. Climate research 21 (3), 219–238.

[36] Smith, T. M., Reynolds, R. W., Peterson, T. C., Lawrimore, J., 2008. Improvements to NOAA's Historical Merged Land–Ocean Surface Temperature Analysis (1880–2006). Journal of climate 21 (10), 2283–2296.

[37] St. George, S., Meko, D. M., Cook, E. R., 2010. The seasonality of precipitation signals embedded within the North American Drought Atlas. Holocene (Sevenoaks) 20 (6), 983–988.

[38] Stahle, D. W., Cleaveland, M. K., Grissino-Mayer, H. D., Griffin, R. D., Fye, F. K., 2009. Cool- and Warm-Season Precipitation Reconstructions over Western New Mexico. Journal of climate 22 (13), 3729–3750.

[39] Trenberth, K. E., 1997. The Definition of El Niño. Bulletin of the American Meteorological Society 78 (12), 2771–2777.

[40] Williams, A. P., Allen, C. D., Macalady, A. K., Griffin, D., Woodhouse, C. A., Meko, D. M., Swetnam, T. W., Rauscher, S. A., Seager, R., Grissino-Mayer, H. D., et al., 2013. Temperature as a potent driver of regional forest drought stress and tree mortality. Nature Climate Change 3 (3), 292–297.

[41] Woodhouse, C. A., Meko, D. M., Griffin, D., Castro, C. L., 2013. Tree rings and multiseason drought variability in the lower Rio Grande

Basin, USA TREE RINGS AND MULTISEASON DROUGHT. Water resources research 49 (2), 844–850.

[42] Wu, B., Zhou, T., Li, T., 2009. Contrast of Rainfall–SST Relationships in the Western North Pacific between the ENSO-Developing and ENSO-Decaying Summers. Journal of climate 22 (16), 4398–4405.

[43] Zhang, Y., Qian, Y., Duliere, V., Salathe, E. P., Leung, L. R., 2012. ENSO anomalies over the Western United States: present and future patterns in regional climate simulations. Climatic change 110 (1-2), 315–346.

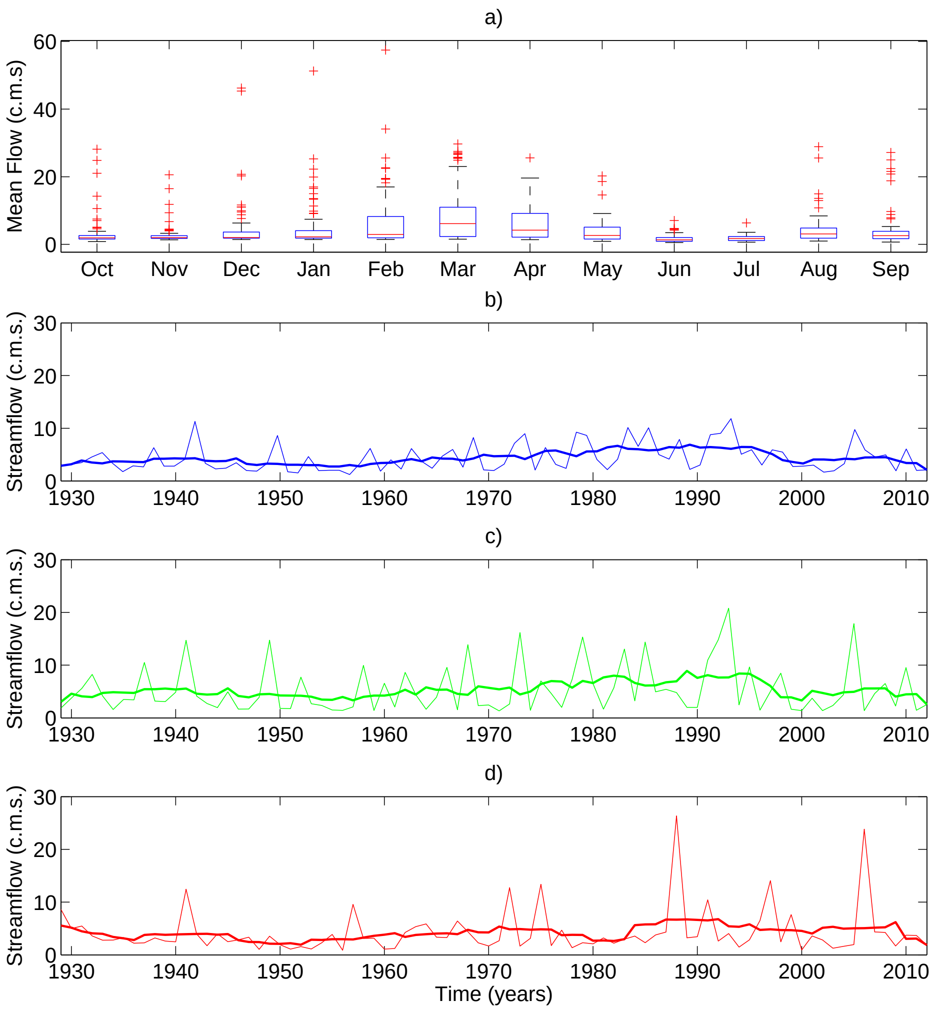

Figure 1: a) Boxplot of monthly flow over the time period 1928 to 2012. For each boxplot, the central mark is the median, the edges of the box are the 25th and 75th percentiles, the whiskers extend to the most extreme data points not considered outliers, and outliers are plotted individually. Timeseries of b) water year (October - September) averaged streamflow, c) December-January-February-March-April-May (DJFMAM) streamflow and d) August-September (AS) streamflow. The thick line shows the ten-year running average.

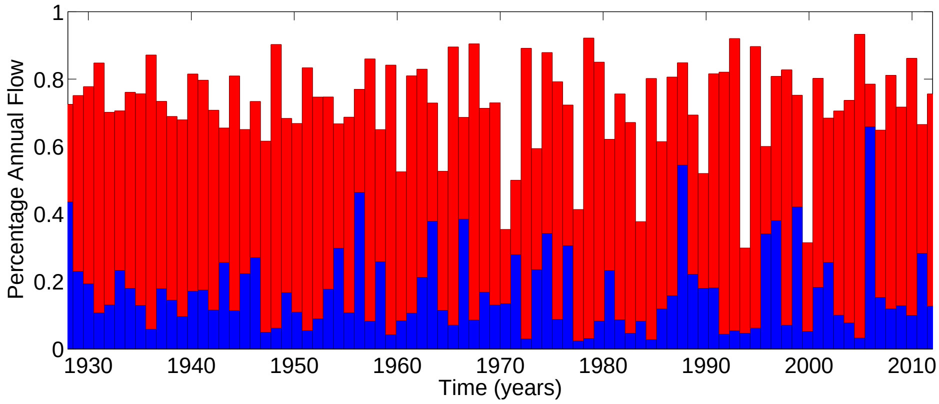

Figure 2: DJFMAM (red bars) and AS (blue bars) streamflow as a percentage of total annual calendar year mean flow for 1928 to 2012. Percentage values are stacked.

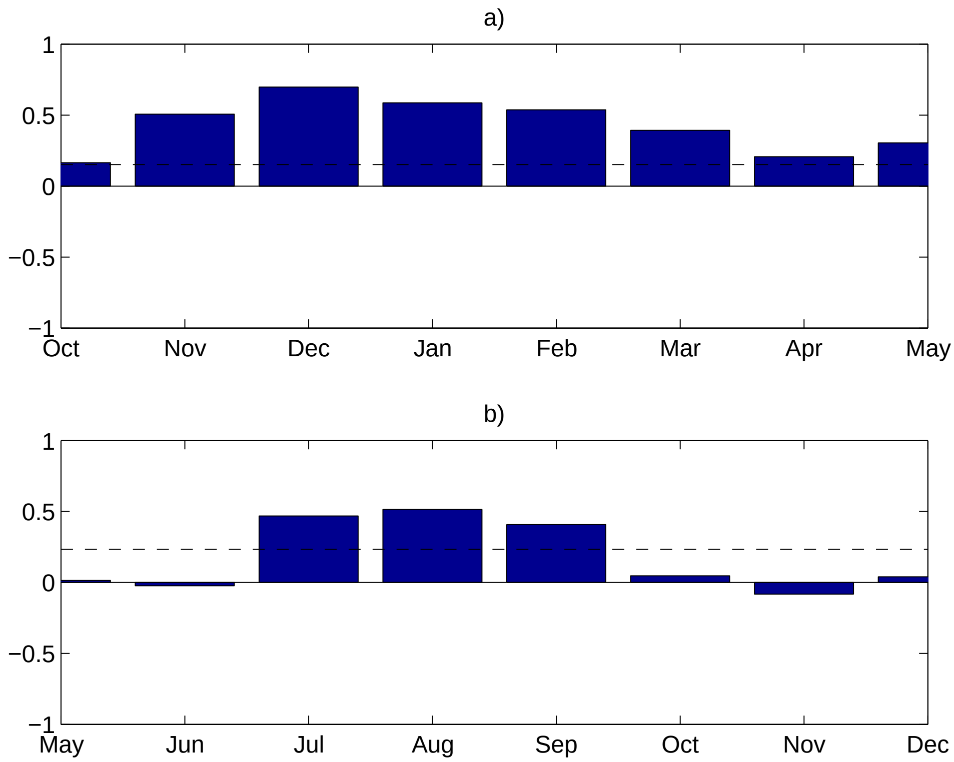

Figure 3: Cross-correlation for a) DJFMAM log-transformed streamflow and b) AS log-transformed streamflow with monthly PRISM precipitation for time period of 1928 to 2012. Dashed line indicates significant at 0.05 level.

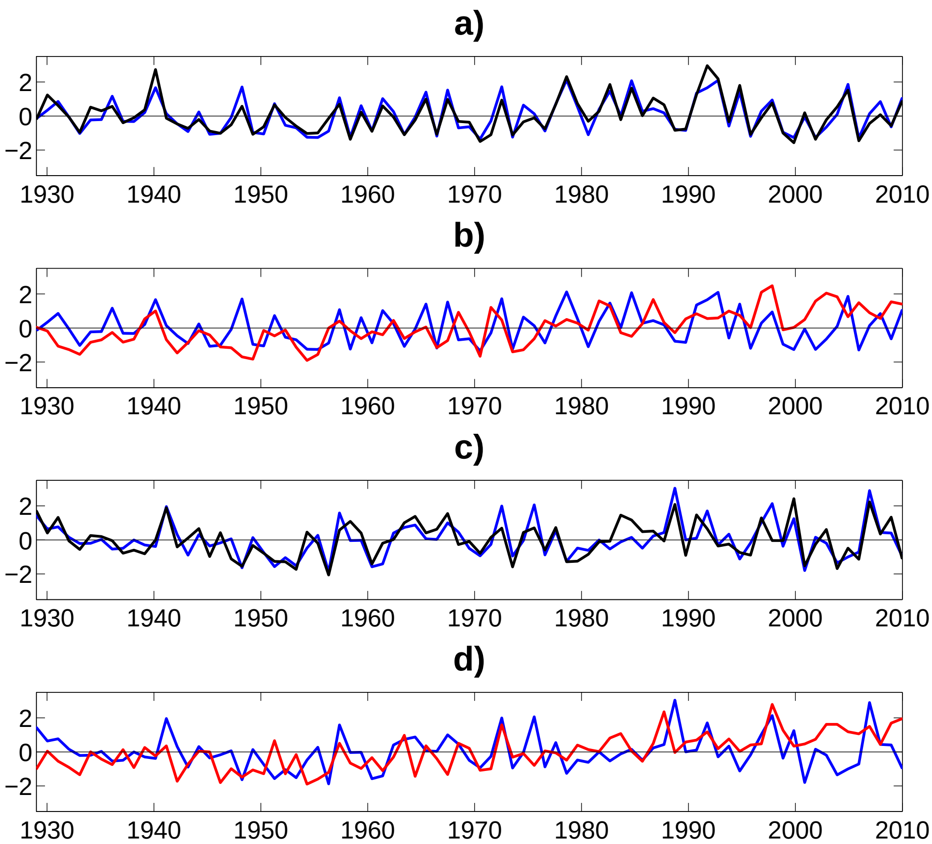

Figure 4: Timeseries of a) DJFMAM log-transformed streamflow and NDJFMAM PRISM precipitation, b) DJFMAM log-transformed streamflow and Niño-4 index for NDJF, c) AS log-transformed streamflow and JAS PRISM precipitation, and d) AS log-transformed streamflow and Niño-4 index for JAS. The data are averaged by year and standardized for time period of 1928 to 2012.

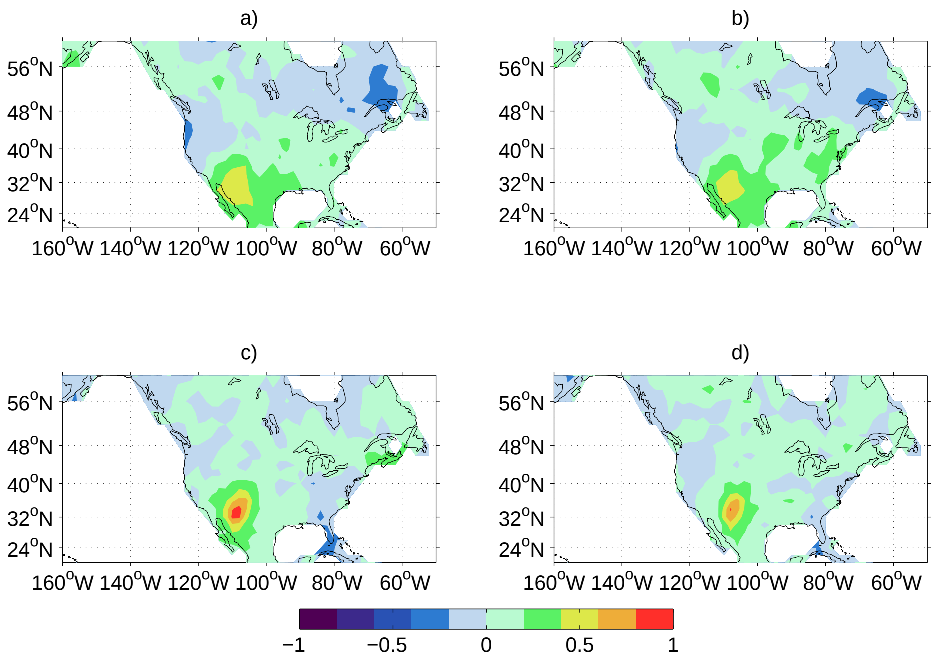

Figure 5: Correlation of North American GPCC precipitation for winter-spring (NDJFMAM) with a) PRISM NDJFMAM precipitation for the Upper Gila Hydrological Unit and b) log-transformed winter-spring (DJFMAM) streamflow and for summer (JAS) with c) PRISM JAS precipitation and d) log-transformed summer (AS) flow.

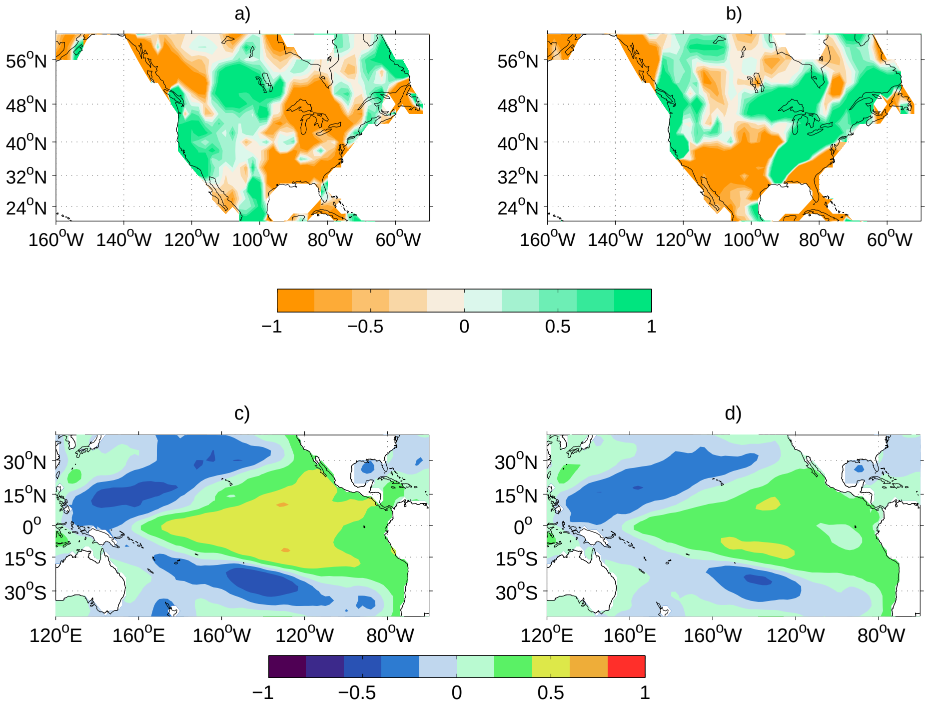

Figure 6: Composites for North American NDJFMAM GPCC precipitation (mm/month) for a) anomalously warm years and b) anomalously cold years in the Nino-4 region (150°W to 160°E and 5°N to 5°S). Warm (cold) years identified by years in which value of the Nino-3.4 index for the DJF season has an anomaly greater (less) than 0.5°C. Correlation of c) NDJFMAM PRISM precipitation over Gila River basin with DJFMAM SST and d) DJFMAM streamflow with DJFMAM SST.

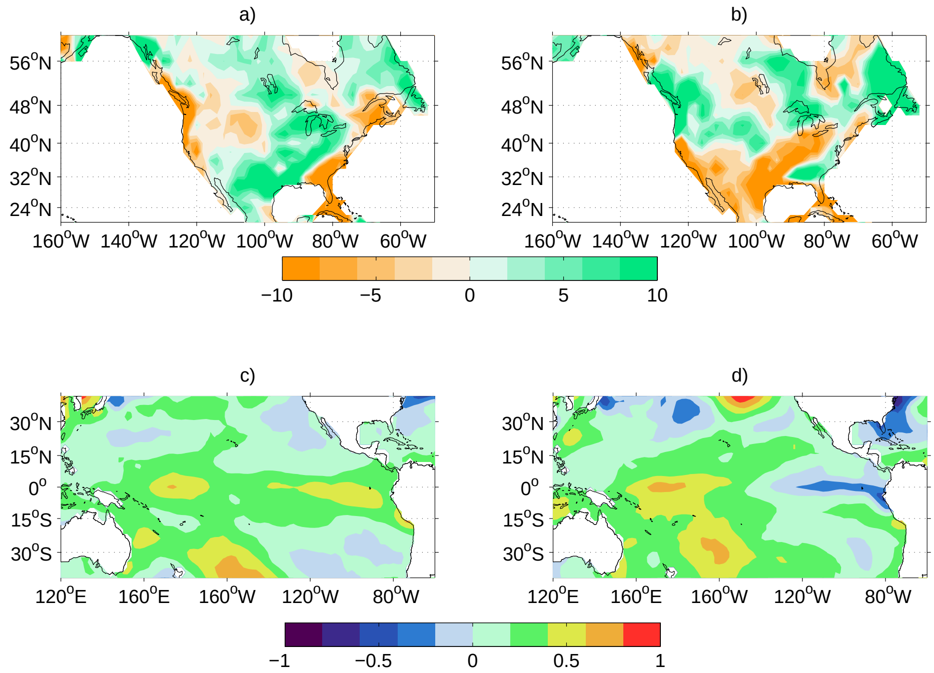

Figure 7: Climate composites for periods of high and low streamflow, defined as high flow for years in which DJFMAM streamflow is greater than 85 percent of the annual flow, and low flows when 15 percent or less for 1928 to 2012. High streamflow composite for a) NDJFMAM GPCC precipitation anomaly and c) DJFMAM SST anomaly, and low streamflow composite for b) NDJFMAM GPCC precipitation anomaly and d) DJFMAM SST anomaly.

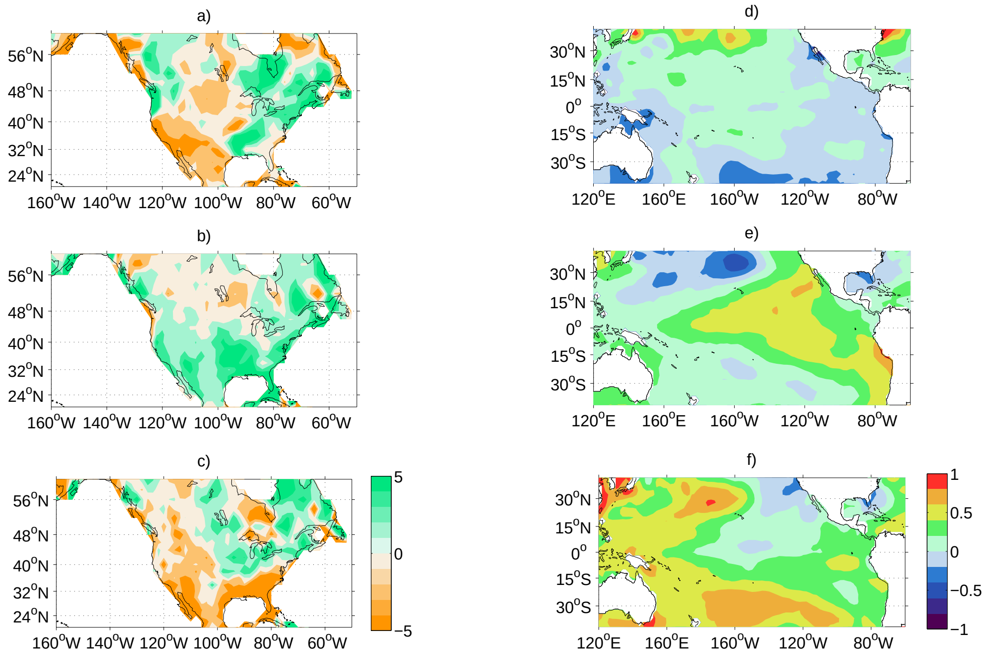

Figure 8: Composite for North American GPCC precipitation during a) 1945-60 period of generally lower flows, b) 1977-97 period of generally higher flows and c) for the most recent decade 1999 to 2012 for NDJFMAM. Composites for SST anomalies during d) 1945-60 period of generally lower flows, e) 1977-97 period of generally higher flows and f) for the most recent decade 1999 to 2012 for DJFMAM over the Pacific.

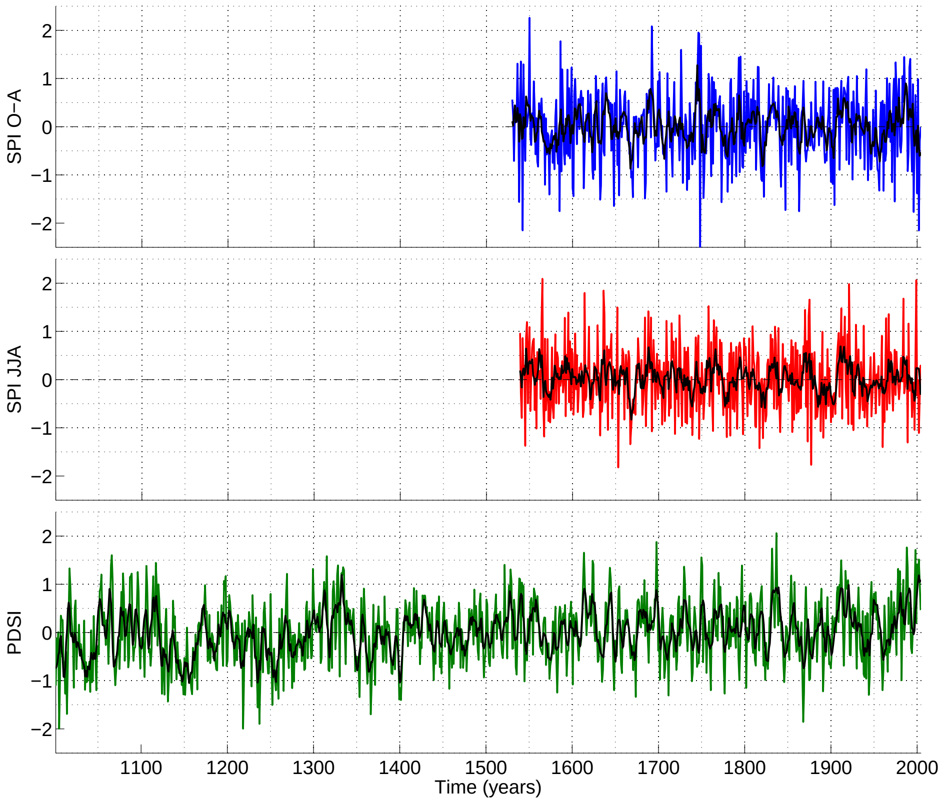

Figure 9: Top time series : reconstructed Standardized Precipitation Index (SPI) (blue line) for 7-months from October to April for 1530 to 2008. Middle time series: Reconstructed SPI (red line) for 7-months from July to August for 1539 to 2008. Bottom time series: Reconstructed PDSI from treering data (green line) from 1000 to 2003. The original annual data are smoothed using a moving average over a five year interval.